

SESF-Fuse: An Unsupervised Deep Model for Multi-Focus Image Fusion

Boyan Ma,^{1,2,3} Xiaojuan Ban,^{1,2,3*} Haiyou Huang,^{1,4*} Yu Zhu^{1,2,3}

¹Beijing Advanced Innovation Center for Materials Genome Engineering, University of Science and Technology Beijing, China.

²School of Computer and Communication Engineering, University of Science and Technology Beijing, China.

³Beijing Key Laboratory of Knowledge Engineering for Materials Science, Beijing, China.

⁴Institute for Advanced Materials and Technology, University of Science and Technology Beijing, China.

Abstract

In this work, we propose a novel unsupervised deep learning model to address multi-focus image fusion problem. First, we train an encoder-decoder network in unsupervised manner to acquire deep feature of input images. And then we utilize these features and spatial frequency to measure activity level and decision map. Finally, we apply some consistency verification methods to adjust the decision map and draw out fused result. The key point behind of proposed method is that only the objects within the depth-of-field (DOF) have sharp appearance in the photograph while other objects are likely to be blurred. In contrast to previous works, our method analyzes sharp appearance in deep feature instead of original image. Experimental results demonstrate that the proposed method achieves the state-of-art fusion performance compared to existing 16 fusion methods in objective and subjective assessment.

Introduction

In recent years, multi-focus image fusion has became an important issue in image processing field. Since the limited DOF of optical lenses, it is difficult to have all objects with quite different distances from the camera to be all-in-focus within one shot (Li et al. 2017). Therefore many researchers devoted to designing algorithm to fuse multiple images of the same scene but with different focus points to create an all-in-focus fused image. The fused image can be used for human or computer operators, and for further image-processing tasks such as segmentation, feature extraction and object recognition.

With the unprecedented success of deep learning, many fusion methods based on deep learning have been proposed. (Liu et al. 2017) first presented a CNN-based fusion method for multi-focus image fusion task. They used gaussian filter to generate synthetic images with different blurred level to train a two-class image classification network. By using such supervised learning strategy, the network could distinguish whether the patch is in focus. After that, DeepFuse (Prabhakar. 2017) has been developed in an unsupervised manner to fuse multi-exposure images. DenseFuse (Li and Wu 2019)

* Corresponding authors: banxj@ustb.edu.cn; huanghy@mater.ustb.edu.cn.

has been designed to fuse infrared and visible images, it utilized unsupervised encoder-decoder network to extract deep features of images and designed L1-norm fusion strategy to fuse two feature maps, and then, the decoder will use fused features to obtain a fused image. The basic assumption behind this approach is that the L1 norm of feature vector for each node represent activity level of that. It can be applied to infrared and visible image fusion task. But for multi-focus task, it is commonly assumed that only the objects within the DOF have sharp appearance in the photograph while other objects are likely to be blurred (Liu et al. 2017). Therefore, we assume that in multi-focus task, what really matter is feature gradient, while feature intensity not.

In order to verify this assumption, we present a fusion method based on unsupervised deep convolutional network. It uses deep feature, which extracted from encoder-decoder network, and spatial frequency to measure activity level. Experimental results demonstrate that the proposed method achieves the state-of-art fusion performance compared to 16 existing fusion methods in objective and subjective assessment.

Our code and data can be found at <https://github.com/MATony/SESF-Fuse>.

The remainder of this paper is organized as follows: In Section II, we provide a briefly review of related works. In Section III, the proposed fusion method is described in detail. The experimental results are shown in Section IV. We conclude the paper in section V.

Related work

In the past decade, various image fusion methods have been presented which could be classified into two groups: transform domain methods and spatial domain methods (Stathaki 2011). The most classical transform domain fusion methods are based on multi-scale transform (MST) theories, such as Laplacian pyramid (LP) (Burt and Adelson 1983), and ratio of low-pass pyramid (RP) (Toet 1989), and wavelet-based ones like discrete wavelet transform (DWT) (Li, Manjunath, and Mitra 1995), and dual-tree complex wavelet transform (DTCWT) (Lewis et al. 2007), and curvelet transform (CVT) (Nencini et al. 2007), and nonsubsampled contourlet transform (NSCT) (Zhang and long Guo 2009), and the

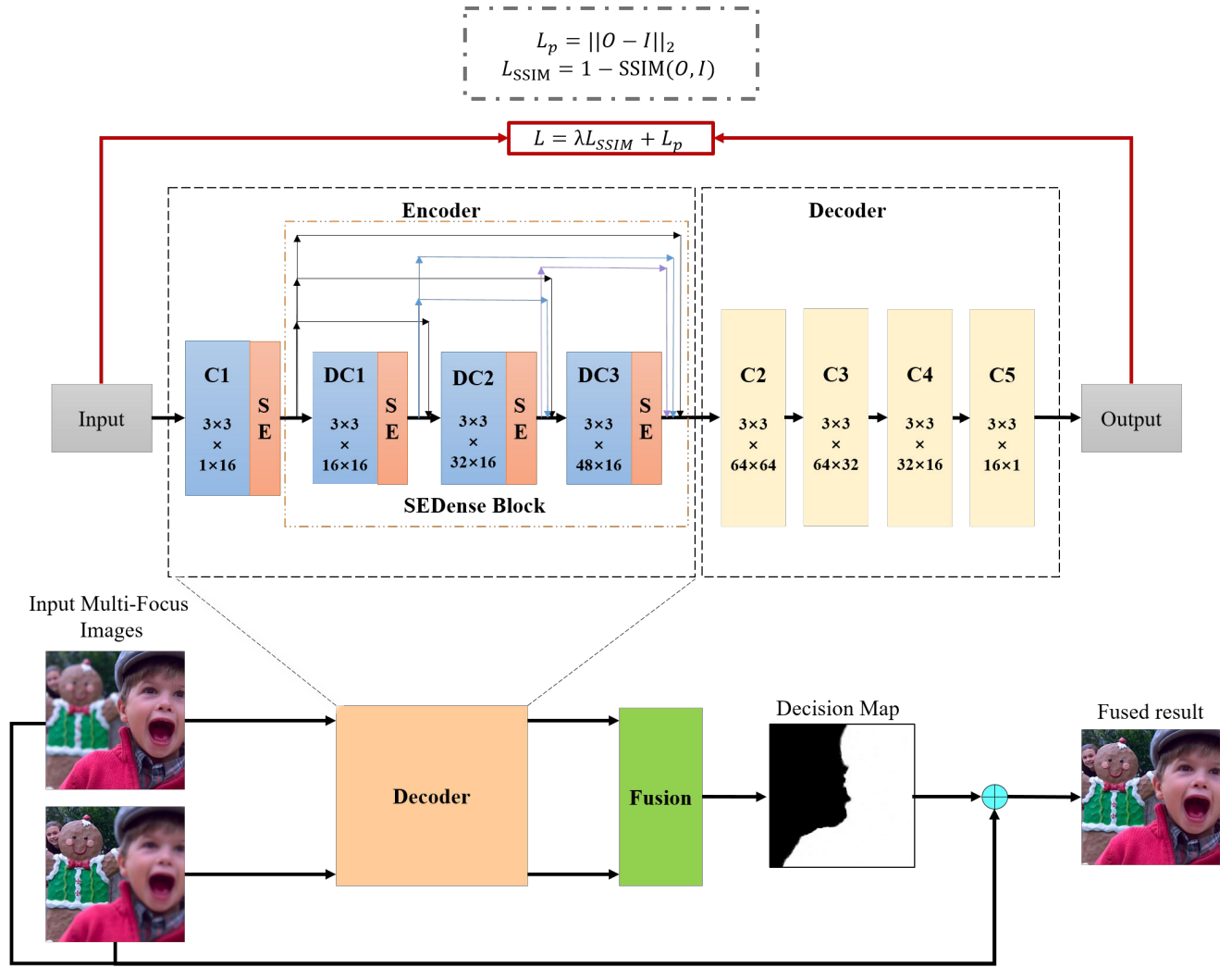


Figure 1: The schematic diagram of proposed algorithm.

sparse representation (SR) (Yang and Li 2010), and image matting based (IMF) (Li et al. 2013). The key point behind these methods is that the activity level of source images can be measured by the decomposed coefficients in a selected transform domain. Obviously, the selection of transform domain plays a crucial role in these methods.

Spatial domain fusion methods measures activity level based on gradient information. Early spatial domain fusion methods used manually fixed size block strategy to calculate activity level, spatial frequency for example (Li, Kwok, and Wang 2001), which usually causes undesirable artifacts. Many improved versions have been proposed on this topic, such as the adaptive block based method (Aslanatas and Kurban 2010) using differential evolution algorithm to obtain a fixed optimal block size. Recently, some pixel-based spatial domain methods based on gradient information have been proposed, such as the guided filtering (GF)-based one (Li, Kang, and Hu 2013), the multi-scale weighted gradient (MWG)-based one (Zhou, Li, and Wang 2014) and the

dense SIFT (DSIFT)-based one (Liu, Liu, and Wang 2015).

With a span of last 5 years, deep convolutional neural network (CNN) has achieved great success in image processing. Some works tried to measure the activity level by high-capacity deep convolutional model. (Liu et al. 2017) first applied convolutional neural network to multi-focus image fusion. (Prabhakar. 2017) performed a CNN-based unsupervised approach for exposure fusion problem, which is so called DeepFuse. (Li and Wu 2019) presented DenseFuse to fuse infrared and visible images, which used encoder-decoder unsupervised strategy to obtain useful features and fused them by L1-norm. Inspired by DeepFuse, we also train our network in unsupervised encoder-decoder manner. Moreover, we apply spatial frequency as fusing rule to obtain activity level and decision map of source images, which is in accord with the key assumption that only the objects within the depth-of-field have sharp appearance.

Method

Overview of Proposed Method

The schematic diagram of our algorithm is shown in Figure 1. We trained an auto-encoder network to extract highly dimensional feature in training phase. Then we calculated the activity level using those deep features at fusion layer in inference phase. Finally, we obtain the decision map to fuse two multi-focus source images. The algorithm presented here only aims at fusing two source images. However, to deal with more than two multi-focus images, it can be straightforwardly fuse them one by one in series.

Extraction of Deep Feature

By getting inspiration from DenseFuse (Li and Wu 2019), we only used encoder and decoder to reconstruct the input image and discarded fusion operation in training phase. After the encoder and decoder parameters are fixed, we use spatial frequency to calculate the activity level from deep features which are obtained by encoder.

As shown in Figure 1, the encoder consists of two parts(C1 and SEDense Block). C1 is 3×3 convolution layer in encoder network. DC1, DC2 and DC3 are 3×3 convolution layers in SEDense block and the output of each layer is connected to every other layer by cascade operation. In order to reconstruct image precisely, there are no pooling layer in network. Squeeze and Excitation (SE) block can enhance spatial encoding by adaptively re-calibrates channel-wise feature responses (Hu, Shen, and Sun 2018), the influence of this structure is shown at the experiment. The decoder consists of C2, C3, C4 and C5, which will be utilized to reconstruct the input image. We minimize the loss function L , which combines pixel loss L_p and structural similarity (SSIM) loss L_{ssim} , to train our encoder and decoder. λ is a constant weight to normalize two loss.

$$L = \lambda L_{ssim} + L_p \quad (1)$$

The pixel loss L_p calculates Euclidean distance between the output(O) and the input(I).

$$L_p = \|O - I\|_2 \quad (2)$$

The SSIM loss L_{ssim} calculates structural differences between O and I . Where $SSIM$ represents to structural similarity operation (Wang et al. 2004).

$$L_{ssim} = 1 - SSIM(O, I) \quad (3)$$

Detailed Fusion Strategy

The detailed fusion strategy is shown in Figure 2. We utilize spatial frequency to calculate initial decision map and applied some commonly used consistency verification methods to remove small errors. Finally, we obtain the decision map to fuse two multi-focus source images.

Spatial Frequency Calculation using Deep Features
Different from L1-norm in DenseFuse, we use feature gradient instead of feature intensity to calculate activity level. Specifically, we apply spatial frequency to handle this task using deep features.

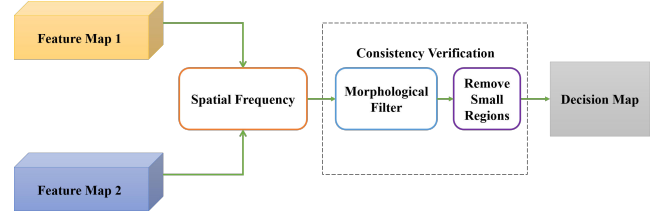


Figure 2: The detailed fusion strategy.

In this paper, the encoder provide high dimensional deep feature for each pixel in an image. However, the original spatial frequency is calculated on gray image with single channel. Thus, for deep feature, we modified the spatial frequency calculation method. Let F represents the deep features driven from encoder block. $F_{(x,y)}$ represents one feature vector, (x, y) refers to the coordinates of these vectors in image. We calculate its spatial frequency with below formulas, where RF and CF are the row and column vector frequency, respectively.

$$RF_{(x,y)} = \sqrt{\sum_{a=-r}^r \sum_{b=-r}^r [F_{(x+a,y+b)} - F_{(x+a,y+b-1)}]^2} \quad (4)$$

$$CF_{(x,y)} = \sqrt{\sum_{a=-r}^r \sum_{b=-r}^r [F_{(x+a,y+b)} - F_{(x+a-1,y+b)}]^2} \quad (5)$$

$$SF_{(x,y)} = \sqrt{\frac{(CF_{(x,y)})^2 + (RF_{(x,y)})^2}{(2r+1)^2}} \quad (6)$$

Where r is radius of kernel. The original spatial frequency is a block-based method, while it is pixel-based in our method. Besides, we apply 'same' padding strategy at the border of feature maps.

Thus, we can compare the spatial frequencies of two corresponding $SF1$ and $SF2$, where k in SFk is index of source image. Then we can get the initial decision map (D) with Eq7.

$$D_{(x,y)} = \begin{cases} 1, & \text{if } SF1_{(x,y)} \geq SF2_{(x,y)} \\ 0, & \text{otherwise} \end{cases} \quad (7)$$

Consistency Verification There may be some small lines or burrs in the connection portions, and some nearby regions may be disconnected by the inappropriate decisions. Thus, an alternating opening and closing operators with a small disk structuring element (De, Chanda, and Chattopadhyay 2006) is applied to process the decision map. In this way, the small lines or burrs could be eliminated, the connection portions of the focused regions could be smoothed, and the nearby regions would be combined as a whole region. We found that, when the radius of the disk structuring element equals to spatial frequency kernel radius, the small

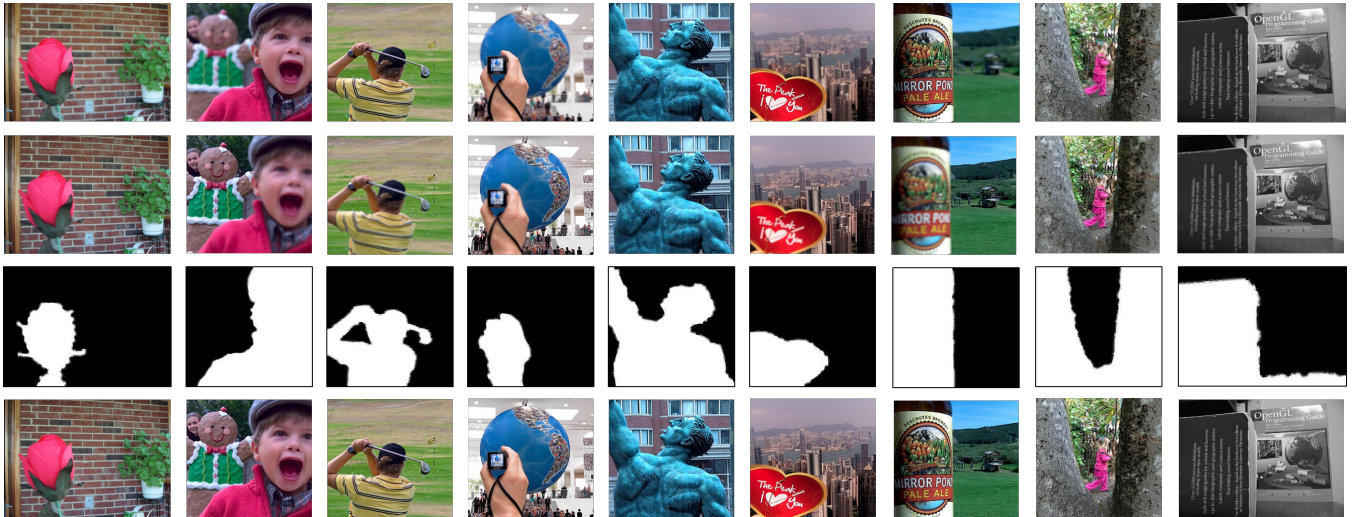


Figure 3: Visualization of fused results. The first row is near focused source image and the second row is far focused source image. The third row is decision map of our method and the final row is fused result.

lines or burrs could be well detected and the nearby regions could be right connected. Beside, we applied the small region removal strategy, which is same with (Liu et al. 2017). Specially, we reversed the region which is smaller than an area threshold. In this paper, the threshold usually set to $0.01 \times H \times W$, where H and W are the height and width of source image, respectively.

Generally, there are some undesirable artifacts around the boundaries between focused and defocused regions. Similar to (Nejati, Samavi, and Shirani 2015), we utilize an efficient edge-preserving filter, guided filter (He, Sun, and Tang 2013), to improve the quality of initial decision map, which can transfer the structural information of a guidance image into the filtering result of the input image. The initial fused image is employed as the guidance image to guide the filtering of initial decision map. In this work, we experimentally set local window radius r to 4 and the regularization parameter ε to 0.1 in guided filter algorithm.

Fusion Finally, by using the obtained decision map D , we calculate the fused result F with the following pixel-wise weighted-average rule. The input images are denoted as Img_k which are pre-registered, where k represents the index of source images. The representative visualization of fused images are shown in Figure 3.

$$F_{(x,y)} = D_{(x,y)} Img1_{(x,y)} + (1 - D_{(x,y)}) Img2_{(x,y)} \quad (8)$$

Experiments

Experimental Settings

In our experiment, we used 38 pairs of multi-focus images as testing set for evaluation, which are publicly available online (Nejati, Samavi, and Shirani 2015; Savić and Babić 2012).

Due to the unsupervised strategy, we first trained the encoder-decoder network using MS-COCO (Lin et al. 2014). In this phase, about 82783 images were utilized as

training set, 40504 images were used to validate the reconstruction ability in every iteration. All of them are resized to 256×256 and transformed to gray scale images. Learning rate was set as 1×10^{-4} and then decreased by a factor of 0.8 at every two epoch. We set $\lambda = 3$ which is same with DenseFuse (Li and Wu 2019) and optimized the objective function with respect to the weights at all network layer by Adam (Kingma and Ba 2015). The batch size and epochs were 48 and 30, respectively. And then we used acquired parameters to perform SF fusion on above testing set.

Our implementation of this algorithm was derived from the publicly available Pytorch framework (Facebook 2019). The networks training and testing were performed on a system using 4 NVIDIA 1080Ti GPU with 44GB memory.

Objective Image Fusion Quality Metrics

The proposed fusion method is compared with 16 representative image fusion methods, which are the laplacian pyramid (LP)-based one (Burt and Adelson 1983), the ratio of low-pass pyramid (RP)-based one (Toet 1989), the non-subsampled contourlet transform (NSCT)-based one (Zhang and long Guo 2009), the discrete wavelet transform (DWT)-based one (Li, Manjunath, and Mitra 1995), dual-tree complex wavelet transform (DTCWT)-based one (Lewis et al. 2007), the sparse representation (SR)-based one (Yang and Li 2010), the curvelet transform (CVT)-based one (Nencini et al. 2007), the guided filtering (GF)-based one (Li, Kang, and Hu 2013), the multi-scale weighted gradient (MWG)-based one (Zhou, Li, and Wang 2014), the dense SIFT (DSIFT)-based one (Liu, Liu, and Wang 2015), the spatial frequency(SF)-based one (Li, Kwok, and Wang 2001), the FocusStack (Wikipedia 2019), the Image Matting Fusion(IMF) (Li et al. 2013), the DeepFuse (Prabhakar. 2017), the DenseFuse (both add and L1-norm fusion strategy) (Li and Wu 2019) and the CNN-Fuse (Liu et al. 2017). In addition, GF, IMF are driven from (Xu 2019) and NSCT, CVT,

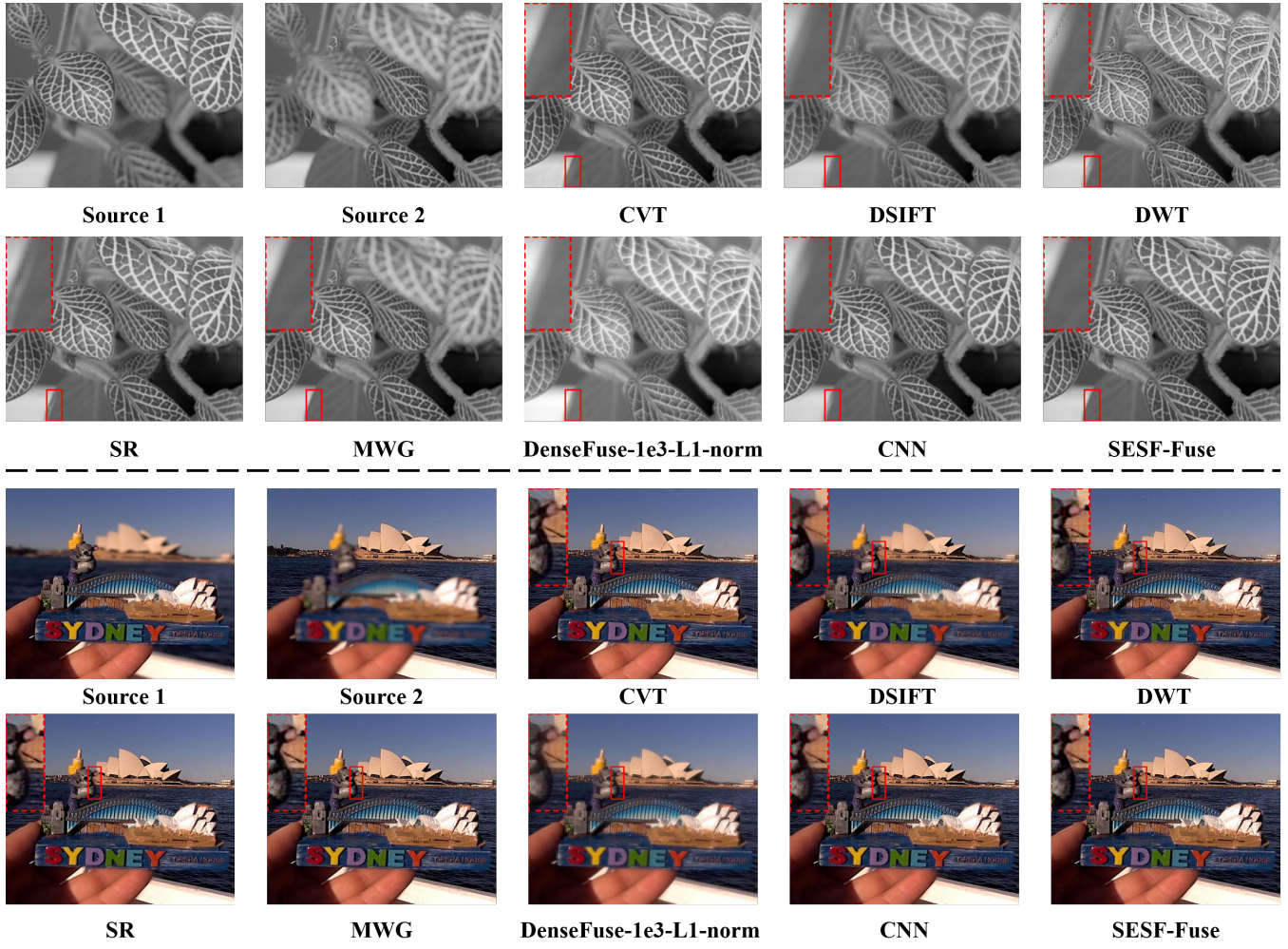


Figure 4: Visualization of different 'leaf' and 'Sydney Opera House' fused results.

DWT, DTCWT, LP, RP, SR and CNN-Fuse from (Liu 2019). In order to access the fusion performance of different methods objectively, we adopt three fusion quality metrics, such as Q_g (Xydeas and Petrovic 2000), Q_m (Peng-wei Wang and Bo Liu 2008) and Q_{cb} (Chen and Blum 2009). For each of the above three metrics, a larger value indicates a better fusion performance. A good comprehensive survey of quality metrics can be found in the article (Liu et al. 2012). For fair comparison, we used default parameters given in the related publications for these metrics and all codes are driven from (Liu 2012).

Ablation Experiments

We first evaluate our methods with different setting to verify our methods. We pick up seven fusion modes to explore the usage of deep features, such as max, abs-max, average, L1-norm, sf, se_sf_dm, and dense_sf_dm. DenseFuse (Li and Wu 2019) investigated add and L1-norm fusion strategy and draw out the conclusion that L1-norm of deep feature could be used to fuse infrared-visible images. They utilized feature

intensity to calculate activity level. We found that feature gradient (calculated by spatial frequency) is suited to multi-focus fusion task. Table 1 shows mean average score with different methods. The bold value denotes the best performance among all fusion modes and the digits within a parenthesis indicates the number of results on which corresponding methods obtain the first place. Se_sf outperforms abs-max, max, average, l1_norm fusion modes in metric evaluation. In addition, even the deep learning have promising representative ability, it can not recover the image perfectly. Thus if we use sf to fuse the deep features and input to decoder and draw out result, the fused result could not completely recover every detail of in-focus region. Therefore, we propose to use deep features to calculate the initial decision map and fuse the original images. As shown in experiment results, the performance of se_sf_dm defeats the se_sf's. Besides, we conduct an experiment to verify the influence of SE architecture (Hu, Shen, and Sun 2018), we have found that the average scores of se_sf_dm in Q_g and Q_m is higher than dense_sf_dm and the first place number of

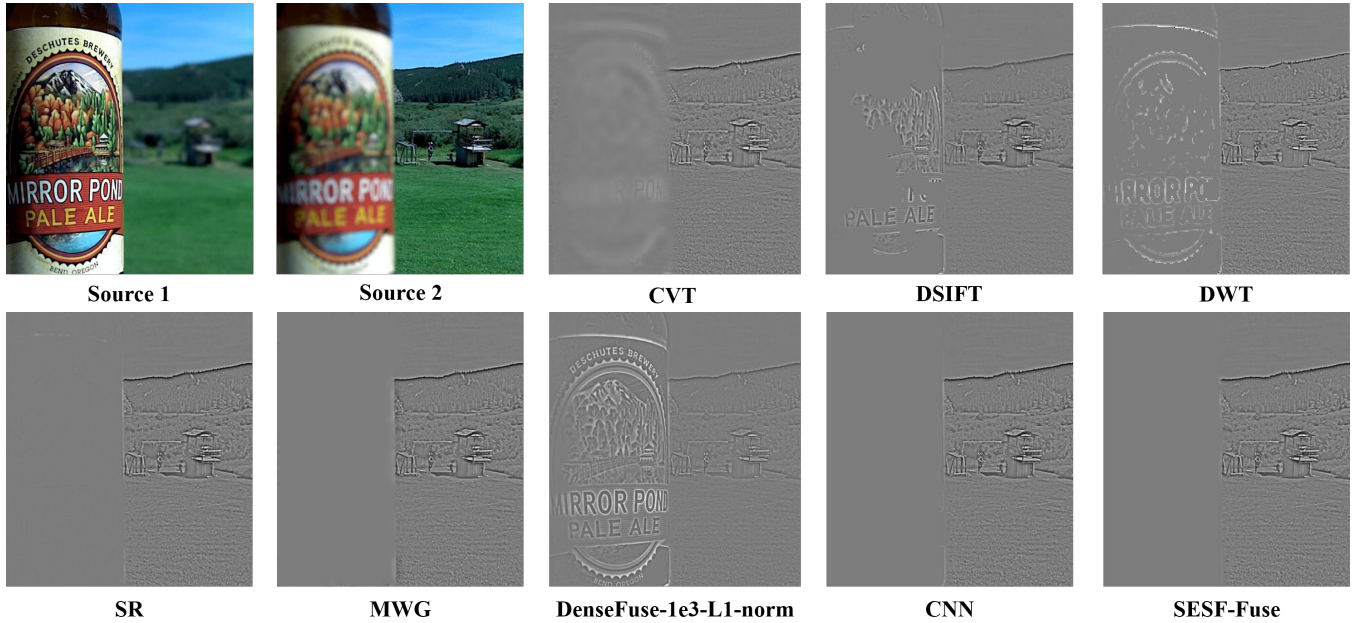


Figure 5: The different image for each 'beer' fused results

se_sf_dm is the highest result. We assume that squeeze-and-excitation structure could dynamic recalibrate feature which shows robust result.

Table 1: Ablation experiments with different setting.

Methods	Q_g	Q_m	Q_{cb}
se_absmax	0.5204(0)	2.4880(0)	0.6019(0)
se_average	0.5033(0)	2.4835(0)	0.5963(0)
se_l1_norm	0.5124(0)	2.4961(0)	0.6020(0)
se_max	0.5059(0)	2.4851(0)	0.5980(0)
se_sf	0.6885(0)	2.7216(2)	0.7526(0)
se_sf_dm	0.7105(25)	2.8886(16)	0.7848(19)
dense_sf_dm	0.7103(13)	2.8872(20)	0.7852(19)

Comparison with other fusion methods

We first compare the performance of different fusion methods based on visual perception. For this purpose, four examples in two manners are mainly provided to exhibit the difference among different methods.

In Figure 4, we visualize two fused example, such as 'leaf' and 'Sydney Opera House' image pairs and their fused results. In each image, a region around the boundary between focused and defocused parts is magnified and shown in the higher left corner. In 'leaf' result, we can see that the border of leaf with different methods. The DWT shows 'serrated' shape and the CVT, DSIFT, SR, DenseFuse, CNN show undesirable artifacts. Besides, for DWT and DenseFuse, the luminance of leaf at right higher corner shows an abnormal increase. And the same region in MWG is out-of-focused, which means that the method can not well detect the focused regions. In 'Sydney Opera

House' result, the ear of Koala located at the border between focused and defocused parts, as we can see that all methods show smooth and blurred result except SESF-Fuse.

To have a better comparison, Figure 5 and Figure 6 show the difference image obtained by subtracting the first source image from each fused image, and the values of each difference image are normalized to the range of 0 to 1. If the near focused region is completely detected, the difference image will not show any information of that. In Figure 5, it is beer bottle. Therefore, the CVT, DSIFT, DWT and DenseFuse-1e3-L1-Norm can not perfectly detect the focused region. The SR, MWG and CNN perform well except that the region at the border of bottle, because we still can see the contour of near focused region. Besides, our SESF-Fuse performs well in both center or border region of near focused regions. In Figure 6, the near focus region is the man. Same with above observation, the CVT, DSIFT, DWT, NSCT, DenseFuse can not perfectly detect the focused region. The MWG and CNN perform well except that the region at the border of the person. Besides, for MWG, the region surrounded by arms is actually far focused region, MWG can not correctly detect here.

Table 2 lists the objective performance of different fusion methods using the above three metrics. We can see that the CNN-based method and the proposed method clearly beat the other 15 methods on the average score of Q_g and Q_{cb} fusion metrics. For Q_g metric, CNN-Fuse and SESF-Fuse achieve comparable performance. However, CNN-Fuse is a supervised method which needs to generate synthetic images with different blurred level to train a two-class image classification networks. By contrast, our network only needs to train an unsupervised model which not used to generate synthetic image data. And for Q_m metric, the average score of

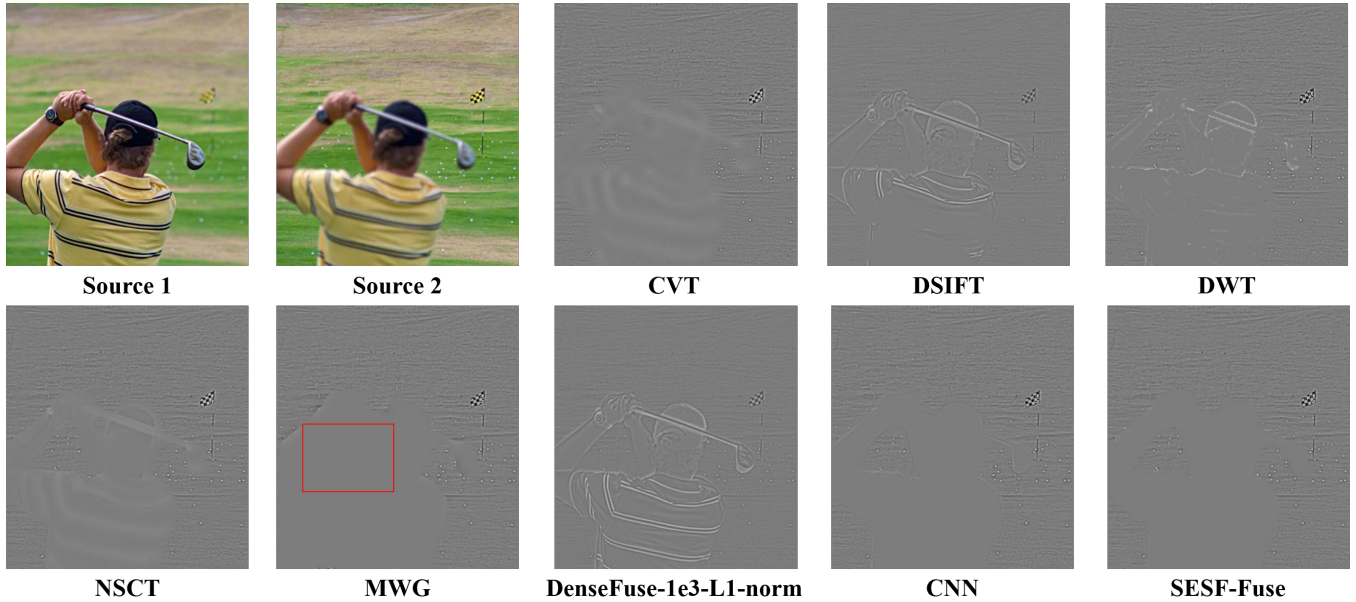


Figure 6: The different image for each 'golf' fused results

Table 2: Comparison with other fusion methods.

Metrics	DeepFuse	FocusStack	SF	DenseFuse_1e3.add	DSIFT	DenseFuse_1e3.II
Q_g	0.4269(0)	0.4709(0)	0.5115(0)	0.5190(0)	0.5267(0)	0.5283(0)
Q_m	2.4618(0)	2.8510(0)	2.8512(0)	2.8530(0)	2.8725(0)	2.8561(0)
Q_{cb}	0.5651(0)	0.6330(0)	0.6024(0)	0.6008(0)	0.6067(0)	0.5972(0)
Metrics	GF	CVT	DWT	IMF	RP	DTCWT
Q_g	0.5631(0)	0.6187(0)	0.6222(0)	0.6324(2)	0.6478(0)	0.6529(0)
Q_m	2.8506(0)	2.9563(0)	2.9465(1)	2.8844(0)	2.9460(0)	2.9583(0)
Q_{cb}	0.7008(3)	0.6908(0)	0.6712(0)	0.7362(4)	0.7101(0)	0.7126(0)
Metrics	NSCT	SR	LP	MWG	CNN-Fuse	SESF-fuse
Q_g	0.6587(0)	0.6686(0)	0.6731(0)	0.6998(0)	0.7102(16)	0.7105(20)
Q_m	2.9592(0)	2.9630(2)	2.9642(8)	2.9615(6)	2.9654(7)	2.8886(14)
Q_{cb}	0.7169(0)	0.7335(0)	0.7352(0)	0.7764(2)	0.7839(9)	0.7848(20)

SESF-Fuse is smaller than LP, however, the first place number of proposed method achieves the highest value which means that it is more robust than other methods.

Considering the above comparisons on subjective visual quality and objective evaluation metrics together, the proposed SESF-Fuse-based fusion method can generally outperform other methods, leading to state-of-the-art performance in multi-focus image fusion.

Conclusion

In this work, we proposed an unsupervised deep learning model to address multi-focus image fusion problem. First, we trained an encoder-decoder network in unsupervised manner to acquire deep feature of input images. And then we utilized these features and spatial frequency to calculate activity level and decision map to perform image fusion. Experimental results demonstrate that the proposed method achieves the promising fusion performance compared to ex-

isting fusion methods in objective and subjective assessment. This paper demonstrated the viability of combination of unsupervised learning and traditional image processing algorithm. Our team will promote this research in subsequent work. Besides, we believe that same strategy could be applied to other image fusion tasks, such as multi-exposure fusion, infrared-visible fusion and medical image fusion.

Acknowledgments

The authors acknowledge the financial support from the National Key Research and Development Program of China (No. 2016YFB0700500), and the National Science Foundation of China (No. 61572075, No. 61702036, No. 61873299, No. 51574027), and Key Research Plan of Hainan Province (No. ZDYF2018139).

References

[Aslantas and Kurban 2010] Aslantas, V., and Kurban, R. 2010. Fusion of multi-focus images using differential evolution algorithm. *Expert Systems with Applications* 37(12):8861 – 8870.

[Burt and Adelson 1983] Burt, P., and Adelson, E. 1983. The laplacian pyramid as a compact image code. *IEEE Transactions on Communications* 31(4):532–540.

[Chen and Blum 2009] Chen, Y., and Blum, R. S. 2009. A new automated quality assessment algorithm for image fusion. *Image and Vision Computing* 27(10):1421 – 1432. Special Section: Computer Vision Methods for Ambient Intelligence.

[De, Chanda, and Chattopadhyay 2006] De, I.; Chanda, B.; and Chattopadhyay, B. 2006. Enhancing effective depth-of-field by image fusion using mathematical morphology. *Image and Vision Computing* 24(12):1278 – 1287.

[Facebook 2019] Facebook. 2019. Pytorch. <https://pytorch.org>.

[He, Sun, and Tang 2013] He, K.; Sun, J.; and Tang, X. 2013. Guided image filtering. *IEEE Transactions on Pattern Analysis and Machine Intelligence* 35(6):1397–1409.

[Hu, Shen, and Sun 2018] Hu, J.; Shen, L.; and Sun, G. 2018. Squeeze-and-excitation networks. In *The IEEE Conference on Computer Vision and Pattern Recognition (CVPR)*.

[Kingma and Ba 2015] Kingma, D. P., and Ba, J. 2015. Adam: A method for stochastic optimization. In *International Conference on Learning Representations*.

[Lewis et al. 2007] Lewis, J. J.; OCallaghan, R. J.; Nikolov, S. G.; Bull, D. R.; and Canagarajah, N. 2007. Pixel- and region-based image fusion with complex wavelets. *Information Fusion* 8(2):119 – 130. Special Issue on Image Fusion: Advances in the State of the Art.

[Li and Wu 2019] Li, H., and Wu, X. 2019. Densefuse: A fusion approach to infrared and visible images. *IEEE Transactions on Image Processing* 28(5):2614–2623.

[Li et al. 2013] Li, S.; Kang, X.; Hu, J.; and Yang, B. 2013. Image matting for fusion of multi-focus images in dynamic scenes. *Information Fusion* 14(2):147 – 162.

[Li et al. 2017] Li, S.; Kang, X.; Fang, L.; Hu, J.; and Yin, H. 2017. Pixel-level image fusion: A survey of the state of the art. *Information Fusion* 33:100 – 112.

[Li, Kang, and Hu 2013] Li, S.; Kang, X.; and Hu, J. 2013. Image fusion with guided filtering. *IEEE Transactions on Image Processing* 22(7):2864–2875.

[Li, Kwok, and Wang 2001] Li, S.; Kwok, J. T.; and Wang, Y. 2001. Combination of images with diverse focuses using the spatial frequency. *Information Fusion* 2(3):169 – 176.

[Li, Manjunath, and Mitra 1995] Li, H.; Manjunath, B.; and Mitra, S. 1995. Multisensor image fusion using the wavelet transform. *Graphical Models and Image Processing* 57(3):235 – 245.

[Lin et al. 2014] Lin, T.-Y.; Maire, M.; Belongie, S.; Hays, J.; Perona, P.; Ramanan, D.; Dollár, P.; and Zitnick, C. L. 2014. Microsoft coco: Common objects in context. In Fleet, D.; Pajdla, T.; Schiele, B.; and Tuytelaars, T., eds., *Computer Vision – ECCV 2014*, 740–755. Cham: Springer International Publishing.

[Liu et al. 2012] Liu, Z.; Blasch, E.; Xue, Z.; Zhao, J.; Laganiere, R.; and Wu, W. 2012. Objective assessment of multiresolution image fusion algorithms for context enhancement in night vision: A comparative study. *IEEE Transactions on Pattern Analysis and Machine Intelligence* 34(1):94–109.

[Liu et al. 2017] Liu, Y.; Chen, X.; Peng, H.; and Wang, Z. 2017. Multi-focus image fusion with a deep convolutional neural network. *Information Fusion* 36:191 – 207.

[Liu, Liu, and Wang 2015] Liu, Y.; Liu, S.; and Wang, Z. 2015. Multi-focus image fusion with dense sift. *Information Fusion* 23:139 – 155.

[Liu 2012] Liu, Z. 2012. Image fusion metrics. <https://github.com/zhengliu6699/imageFusionMetrics>.

[Liu 2019] Liu, Y. 2019. Image fusion. <http://www.escience.cn/people/liuyu1/Codes.html>.

[Nejati, Samavi, and Shirani 2015] Nejati, M.; Samavi, S.; and Shirani, S. 2015. Multi-focus image fusion using dictionary-based sparse representation. *Information Fusion* 25:72 – 84.

[Nencini et al. 2007] Nencini, F.; Garzelli, A.; Baronti, S.; and Alparone, L. 2007. Remote sensing image fusion using the curvelet transform. *Information Fusion* 8(2):143 – 156. Special Issue on Image Fusion: Advances in the State of the Art.

[Peng-wei Wang and Bo Liu 2008] Peng-wei Wang, and Bo Liu. 2008. A novel image fusion metric based on multi-scale analysis. In *2008 9th International Conference on Signal Processing*, 965–968.

[Prabhakar. 2017] Prabhakar, R. 2017. Deepfuse: A deep unsupervised approach for exposure fusion with extreme exposure image pairs. In *The IEEE International Conference on Computer Vision (ICCV)*.

[Savić and Babić 2012] Savić, S., and Babić, Z. 2012. Multi-focus image fusion based on empirical mode decomposition. In *19th IEEE International Conference on Systems, Signals and Image Processing (IWSSIP)*.

[Stathaki 2011] Stathaki, T. 2011. *Image fusion: algorithms and applications*. Elsevier.

[Toet 1989] Toet, A. 1989. Image fusion by a ratio of low-pass pyramid. *Pattern Recognition Letters* 9(4):245 – 253.

[Wang et al. 2004] Wang, Z.; Bovik, A. C.; Sheikh, H. R.; and Simoncelli, E. P. 2004. Image quality assessment: from error visibility to structural similarity. *IEEE Transactions on Image Processing* 13(4):600–612.

[Wikipedia 2019] Wikipedia. 2019. Focus stacking. <https://github.com/cmcguinness/focusstack>.

[Xu 2019] Xu, K. 2019. Image fusion. <http://xudongkang.weebly.com/index.html>.

[Xydeas and Petrovic 2000] Xydeas, C. S., and Petrovic, V.

2000. Objective image fusion performance measure. *Electronics Letters* 36(4):308–309.

[Yang and Li 2010] Yang, B., and Li, S. 2010. Multifocus image fusion and restoration with sparse representation. *IEEE Transactions on Instrumentation and Measurement* 59(4):884–892.

[Zhang and long Guo 2009] Zhang, Q., and long Guo, B. 2009. Multifocus image fusion using the nonsubsampled contourlet transform. *Signal Processing* 89(7):1334 – 1346.

[Zhou, Li, and Wang 2014] Zhou, Z.; Li, S.; and Wang, B. 2014. Multi-scale weighted gradient-based fusion for multi-focus images. *Information Fusion* 20:60 – 72.